Atomic-Site-Specific Analysis on Out-of-Plane Elasticity of Convexly Curved Graphene and Its Relationship to sp^2 to sp^3 Re-Hybridization

Makoto Ashino [1,2,*] and Roland Wiesendanger [2]

[1] Department of Electrical & Electronic Engineering, Kanazawa Institute of Technology, Nonoichi 921-8501, Japan
[2] Department of Physics, University of Hamburg, 20355 Hamburg, Germany; wiesendanger@physnet.uni-hamburg.de
[*] Correspondence: mashino@neptune.kanazawa-it.ac.jp; Tel.: +88-76-248-1100

Abstract: The geometry of two-dimensional crystalline membranes is of interest given its unique synergistic interplay with their mechanical, chemical, and electronic properties. For one-atom-thick graphene, these properties can be substantially modified by bending at the nanometer scale. So far variations of the electronic properties of graphene under compressing and stretching deformations have been exclusively investigated by local-probe techniques. Here we report that the interatomic attractive force introduced by atomic force microscopy triggers "single"-atom displacement and consequently enables us to determine out-of-plane elasticities of convexly curved graphene including its atomic-site-specific variation. We have quantitatively evaluated the relationship between the out-of-plane displacement and elasticity of convexly curved graphene by three-dimensional force field spectroscopy on a side-wall of a hollow tube with a well-defined curvature. The substantially small intrinsic modulus that complies with continuum mechanics has been found to increase significantly at atomically specific locations, where sp^2 to sp^3 re-hybridization would certainly take place.

1. Introduction

There is a long-standing discussion [1–3] about how the properties of conformal elastic two-dimensional (2D) crystalline membranes [4,5] are affected by geometry [6,7]. Whereas three-dimensional (3D) crystals cannot exceed a few percentage points of elastic strain, the 2D crystalline membranes can sustain a much larger strain of tens of percent, leading to peculiar responses of their properties [8,9]. The flexible elastic 2D membranes can thereby assume the shape of arbitrary two-dimensional manifolds [10,11]. The first ultimate 2D crystalline membrane is graphene, a monolayer of carbon atoms arranged in a honeycomb lattice, capable of being isolated from a layered crystal, graphite, known as one of the most inert materials [4,12,13]. Beyond the ideal continuum models of the pristine 2D graphene membrane based on the Dirac equation, in which charge carriers act as relativistic fermions with massless characteristics [14], a great deal of attention has been paid to its stability in 3D space [15–18]. Incidentally, the study of quantum electrodynamics in curved space (i.e., a curved two-dimensional manifold [10]) realized by a controllable bending of graphene provides opportunities to examine even cosmological problems [12,19–21].

Although the carbon atoms of the graphene honeycomb lattice are chemically inert due to π-conjugation, it has been reported that atomic hydrogen can be chemically bonded to each carbon

atom resulting in graphane [22]. The charge inhomogeneity revealed in the intrinsic graphene can be attributed to its inherent geometry of warping or rippling [12,23]. It was theoretically [24] and experimentally [25] shown that the hydrogen affinity can be enhanced on the convexly curved areas of rippled graphene. A possible pathway of initiating or accelerating the reactions is the use of force [26] to deform a graphene sheet along a specific direction of the reaction coordinate, such as the out-of-plane direction, and especially to enhance its local curvature. Such mechanical deformations can induce local symmetry breaking, which destabilizes electronic bonding [26,27] and possibly makes the graphene prone to chemical reactions. However, experimental evidence for those possibilities is so far lacking.

Here we report that the attractive force field introduced by the local probe technique triggers out-of-plane relaxation of the individual carbon atoms (resulting in the local acumination of ripples) of convexly curved graphene and consequently enables us to determine its out-of-plane elastic properties including its atomistic variation. Thorough characterizations were carried out on a side wall of a hollow nanotube, a rolled-up form of graphene, by 3D force field spectroscopy based on atomic force microscopy (AFM: home-build) [28]. Three-dimensional force-field mapping reveals an atomically specific local enhancement of out-of-plane elasticity beyond the substantially small elastic moduli resulting from the flexible elastic 2D membrane of one-atom-thick graphene. We found that, while the continuum mechanics would still be available at the hollow site of the honeycomb lattice, out-of-plane elasticity would be significantly enhanced at the individual carbon atom site, where the carbon atom more favorably moves out of plane toward the probe-tip apex against the bending rigidity (softening or vanishing of the bending rigidity, as described in [21], probably takes place). Our findings suggest that the tension applied by attractive forces in AFM would provide insight into the atomically specific properties of graphene mechanics and provide experimental evidence of local-curvature-induced sp^2 to sp^3 re-hybridization, which results in a local enhancement of chemical reactivity.

2. Materials and Methods

A single-walled carbon nanotube (SWNT) can be utilized to evaluate the out-of-plane mechanical properties of convexly curved graphene because its side wall, having a certain curvature, would be regarded as a well-defined analogue of free-standing curved graphene. Indeed, SWNTs consist of single-layered graphene, rolled-up to a hollow core with a uniform radius of curvature at the nanometer scale. Figure 1 shows a surface topography of SWNT with a well-defined radius $R_o = 6.9 \pm 0.1$ Å [28,29], imaged by AFM with atomic resolution. The topography, representing slender and convexly curved features, has been obtained in an ultrahigh vacuum ($< 10^{-8}$ Pa) at low temperature (< 15 K) under frequency-modulation (FM) feedback control to maintain a constant frequency shift $\Delta f = -65.3$ Hz of the cantilever resonant oscillation ($f_o \cong 159$ kHz). Owing to the relationship between Δf and interaction forces F formulated by Sader et al. [30], the FM-feedback control keeps a constant attractive force continuously acting on the tip apex over the sample surfaces. Atomically resolved features result from detecting highly sensitively interatomic forces, which has been realized by scanning the AFM tip with an atomically sharp silicon (Si) apex over the topmost part of a hollow tube. The radius of the tip-apex curvature used in our study was estimated to be $R_t = 5.8 \pm 0.6$ Å by a deconvolution method for the sections in 3D topographies [31]. The atomically resolved AFM imaging enables us not only to confirm surface cleanliness and to determine the chirality of curved graphene but also to characterize its chemical and mechanical properties at atomically specific sites [28,32,33].
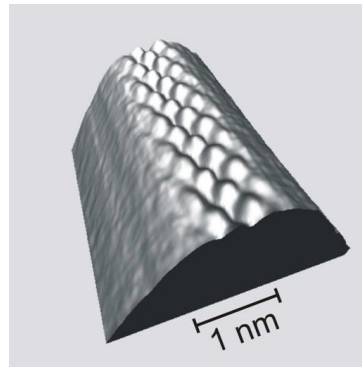
Figure 1. Atomic-resolution AFM topography of a single-walled carbon nanotube (SWNT) with a well-defined radius $R_o = 6.9 \pm 0.1$ A in 3D view. The image size is $3 \times 3 \times 1$ nm^3. The atomically resolved depressing and protruding features are observed on the topmost part of a convexly curved surface.

In three-dimensional (3D) force field spectroscopy (3D-FFS), tip-sample interaction forces are measured by recording $\Delta f(x, y, z)$ and converting that to $F(x, y, z)$. At every recording point (x, y) over the sample surface, the tip-sample distance z is regulated to attain the same Δf value and consequently to obtain the surface topography as in the case of previous imaging with atomic resolution [28,32,33]. Acquisition of the atomically resolved topography, which also took place during the 3D-FFS measurement, allows for an atomic-site-specific analysis of interaction forces. In our study, as illustrated in Figure 2a,b, the 3D-FFS measurement was carried out over the topmost part of the SWNT where the surface topography (in 3D view [34]) in the upper panel of Figure 2a was obtained immediately beforehand (for a detailed experimental set-up, see [28]). The regulating-point image in the lower panel shows almost the same features as represented in the upper panel. By comparing between the upper and lower images, we found that, while the adjacent two sites marked by C1 and C2 represent depressing features in the surface topography, the H-site represents a protruding feature. The vertically sectional force map along the horizontal line, indicated by a pair of counter arrows, even represents an atomic-scale contrast of the total interaction forces F_{total}, as shown in Figure 2c, where the positions corresponding to the C1, C2, and H sites in Figure 2a are indicated by pairs of arrows and dashed lines, respectively. The vertical distance z relationships of the total forces $F_{\text{total}}(z)$ along the three vertical dashed lines in Figure 2c are plotted in Figure 2d. As for the contrast of the vertically sectional force map in Figure 2c, the difference among force vs. distance z relationships in Figure 2d becomes remarkably in close proximity to the sample surface. The short-range forces $F_{\text{sht}}(z)$ contributing to the atomic-scale contrast and consequently to the interatomic forces, i.e., $F_{\text{sht}}(z) = F_{\text{int}}(z)$ are derived by subtracting their common long-range contribution, drawn by a blue-colored solid line in Figure 2d.
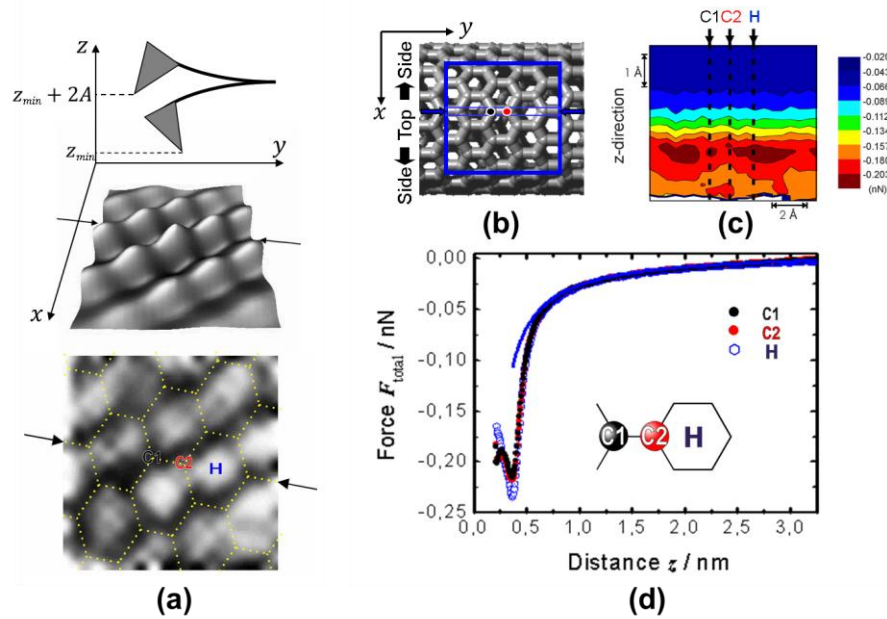
Figure 2. (**a**) Schematic illustration of a 3D-FFS measurement over the topmost 1×1 nm^2 area of the SWNT as depicted in (**b**). The upper (3D) and lower (2D) images in (a) are the surface topographies obtained before and during the measurement, respectively. The elongation of the honeycomb structure (dotted line) can be explained geometrically by assuming a point-like tip scanning across a curved surface (see text). (**c**) 2D force field map obtained along the line indicated by a pair of counter arrows in (a). (**d**) Force vs. distance relationships along the dashed lines in (c), corresponding the C1, C2, and H sites marked in (a) and (c) (for details see text).

3. Results

3.1. Interatomic Forces Obtained at Atomically Specific Sites

As shown in Figure 2d, the difference between the forces at the depressing (C1 and C2) sites is negligibly small even in close proximity. Thereby the interatomic forces $F_{int}(z)$ obtained at the C and H sites representing the depressing and protruding features in Figure 2a are respectively averaged and plotted in Figure 3a. By comparison between the simultaneously measured 3D force and damping fields [32,35], we found that the foremost atom of the tip apex contributes mainly to the elastic interactions with the topmost carbon (C) atoms of the central ridge. The 3D damping fields specify the locations where the tip apex inelastically interacts with the sample surface. As described in [33], such inelastic signals are completely absent in the 3D damping fields, meaning that the interatomic interactions are purely elastic over the central ridge of the convexly curved graphene. Consequently, the $F_{int}(z)$ plots in Figure 3a represent atomically specific features in its elasticity. In such a situation, as shown by the solid curves in Figure 3a, the interatomic forces $F_{int}(z)$ have been successfully described either by Lennard–Jones force or by its "hybrid" with a Morse force, corresponding to the sp^2 and sp^3 hybridizations, as follows:

$$F_{int}(1/R,\, z_{int}) = g(1/R) \cdot F_0^{sp^2}(z_{int}) + [1 - g(1/R)] \cdot F_0^{sp^3}(z_{int}), \tag{1}$$

$$F_0^{sp^2}(z_{int}) = \frac{12 U_o^{sp^2}}{z_o} \left[\left(\frac{z_o}{z_{int}} \right)^{13} - \left(\frac{z_o}{z_{int}} \right)^{7} \right], \tag{2}$$

$$F_0^{sp^3}(z_{int}) = \frac{2 U_o^{sp^3}}{\lambda} \left\{ exp\left[-2\left(\frac{z_{int} - z_o}{\lambda} \right) \right] - exp\left[-\left(\frac{z_{int} - z_o}{\lambda} \right) \right] \right\}, \tag{3}$$

where the curvature parameter $g(1/R)$ is defined as

$$g(1/R) = \left(1 - \frac{1/R}{1/R_t}\right)^{\alpha}. \tag{4}$$

$1/R_t$ is the reference constant, and α is a positive number. It should be noted that the lower solid curve (blue) in Figure 3a was obtained only by Equation (2), corresponding to the Lennard–Jones force. On the other hand, the upper solid curve (Red) in Figure 3a was obtained by adopting $U_o^{sp^2} \equiv 10.2$ meV and $U_o^{sp^3} \equiv 1.41$ eV [36] in Equations (2) and (3), and by adopting $1/R_t \equiv 1.724$ nm^{-1} and $\alpha \equiv 0.027$ in Equation (4), respectively. The well-depth parameters $U_o^{sp^2}$ and $U_o^{sp^3}$ were obtained by adapting the Lennard–Jones parameter for Ar atoms [37] to those for Si and C atoms, and by adapting the Si − C binding energy for single-layered graphene [36], respectively. The reference constant $1/R_t$ was based on the radius of curvature $R_t = 5.8$ *A* of the tip apex in our study. The decay length parameter λ in the Morse force was individually estimated to find an excellent fit to the experimental-data plots. From the above, the lower (blue) and upper (red) solid curves exhibiting excellent fits were respectively obtained by taking the Lennard–Jones force only and its "hybrid" with the Morse force into account. Consequently, the $F_{int}(z)$ plots in Figure 3a obtained at the respective C and H sites representing the depressing and protruding features in Figure 2 demonstrate obviously different elasticities, which might be originating from different atomic lattice sites, namely the carbon atom and hollow sites of the honeycomb graphene lattice, respectively. It should be noted that the elongation of the honeycomb structure, indicated by the dotted lines in Figure 2a, can be geometrically explained by assuming a point-like tip scanning across a curved surface [38]. After correction of this image artefact, the depressing features surrounding each protruding feature show good agreement with the regular hexagon of the nearest neighbor C − C distance (1.421 *A*) [39].
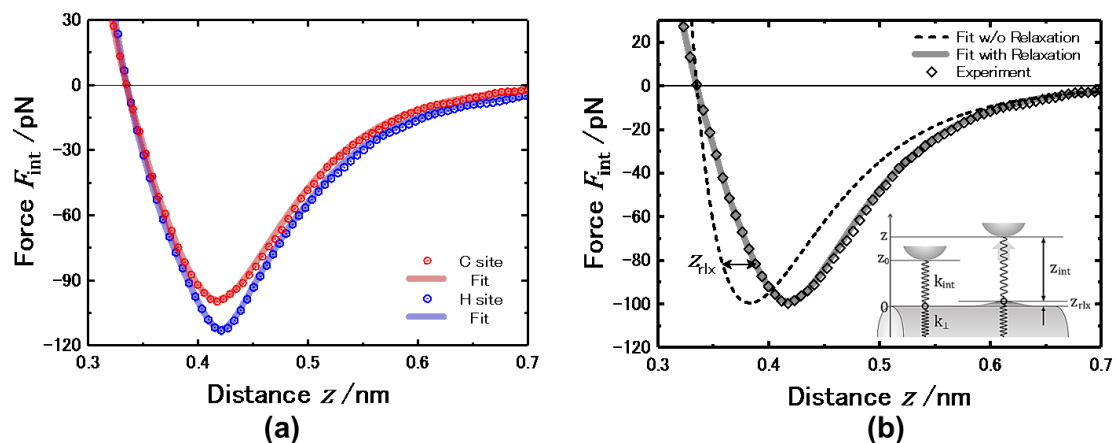

Figure 3. (**a**) Interatomic force F_{int} vs. vertical distance z relationship at atomically specific C and H sites over the topmost part of convexly curved graphene. The C and H sites are respectively corresponding to the atomically specific sites representing depressing and protruding features in the topography image (i.e., the lower panel in Figure 2a) obtained during the 3D-FFS measurement. The interatomic forces F_{int} obtained at those sites were respectively averaged and plotted with the simulation curves (solid lines). (**b**) The relationship between the simulation curves of solid and dashed lines obtained with and without taking relaxation into account, respectively. Those simulation curves are drawn together with the experimental-data plots obtained at the C site. The out-of-plane relaxation of the closest carbon atom due to the interatomic attractive force acting to the tip-apex atom is schematically illustrated in the inset of (b).

3.2. Quantitative Evaluation of Out-of-Plane Elastic Stiffness

Since the out-of-plane stiffness of one-atom-thick graphene should be extremely small [40,41], the interatomic attractive force acting on the convexly curved graphene in close proximity is expected to make the closest carbon atom relaxed, as depicted in the inset of Figure 3b. The vertical z coordinate of the carbon atom was set to zero when the tip-apex atom is separated only by the equilibrium $z_o (= 3.35\ A)$ distance. By adopting the "relaxed" displacement z_{rlx} of the carbon atom, corresponding to the relaxation due to the interatomic attractive forces applied by the tip-apex atom, the interatomic distance z_{int} between those two atoms is properly described as $z_{int} = z - z_{rlx}$. The simulation curve (solid line), obtained by taking such relaxations of the carbon atom into account, shows excellent agreement with the experimental-data plots in Figure 3b. On the other hand, the simulation curve (dashed line), obtained by assuming that the carbon atom rigidly stays at its position without any relaxation, shows large deviations in the vertical z direction from the experimental-data plots.

Using the "relaxed" displacement z_{rlx} of the carbon atom, the interatomic forces acting on the tip-apex atom can be expressed as $F_{int} = k_\perp \cdot z_{rlx}$ (or $F = k_E \cdot z_{lft} + k_D \cdot z_{rlx}^2 + k_C \cdot z_{rlx}^3 + \cdots$) because their interaction was found to be elastic, as mentioned above. The so-called "out-of-plane" elastic stiffness $k_\perp$ of the convexly curved graphene was expected to vary with the local increment of the curvature $\Delta(1/R)_{rlx}$, with a linear correlation to z_{rlx}, as described in [33]. Since Hooke's law applies for small displacement Δz_{rlx}, the "out-of-plane" elastic stiffness $k_\perp$ can be derived from the infinitesimal force change dF_{int} for the infinitesimal displacement dz_{rlx} as $k_\perp = dF_{int}/dz_{rlx}$. The relationship of the $k_\perp$ values with the relaxed displacement z_{rlx}, which were derived from the interatomic forces F_{int} obtained at the C and H sites (see Figure 3), is shown in Figure 4a. By comparing the variations of both sites, we found that for the H site the variations are relatively small and almost constant except for the displacement z_{rlx} near the maximal z_{rlx}^{max}. On the other hand, for the C site, although the variations are found to be almost constant around small displacements ($z_{rlx} < 0.015$ nm), they increase significantly until the maximal z_{rlx}^{max}.
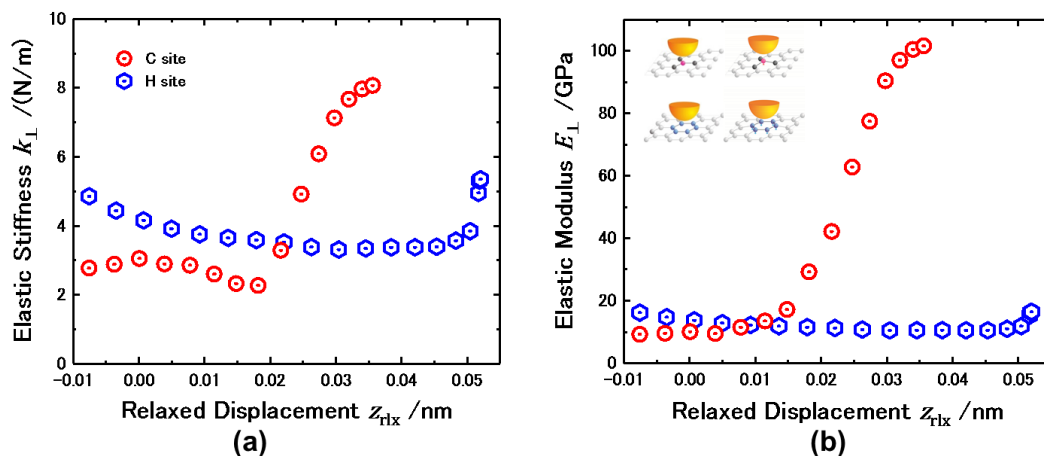

Figure 4. Quantitative relationship of (**a**) out-of-plane elastic stiffness $k_\perp$ and (**b**) elastic modulus $E_\perp$ at the atomically specific C and H sites of the convexly curved graphene with the relaxed displacement z_{rlx} in the vertical direction due to tip-sample attractive interaction. The effective area of the interatomic forces acting between the tip-apex atom and the C and H sites are schematically illustrated in the inset of (**b**).

4. Discussions

Here we discuss why the out-of-plane elastic stiffness $k_\perp$ obtained at the C site is obviously different from the H site. The surface topography (Figure 2a) represents the depressing features at the C site and in contrast the protruding features at the H site. The correction of the upper and

lower panels of Figure 2a taking the image artefact into account show that the depressing C sites are regularly hexagonal surrounding the protruding H sites. Over the individual carbon atoms of graphene, the π-orbitals forming a reciprocal weak bond (i.e., π-bond) predominantly contribute to the attractive forces acting on the tip-apex atom, unless any electron-transfer reactions take place [17,18,42]. In case the tip-apex atom is located over the carbon atom site of the honeycomb lattice, the closest atom and three nearest neighbors additively contribute to such "non-bonding" interactions. On the other hand, above the hollow site, the tip-apex atom interacts with the surrounding six carbon atoms. Under the inverse power law, the interatomic attractive forces acting on the tip-apex atom at the hollow site get stronger than those at the carbon atom site. Consequently, topographic images obtained under feedback control to keep a constant force should represent protruding features at the hollow sites and depressing features at the carbon atom sites. Therefore, the plots obtained at the C and H sites in Figure 4a correspond to the variation of out-of-plane elastic stiffness $k_\perp$ at the carbon atom site and the hollow site, respectively.

　　　The "relaxed" displacement z_{rlx} of the C atom enables us to evaluate the out-of-plane Young's modulus $E_\perp$ because it can be defined as $E_\perp = (F/A)/[(\Delta z/2)(1/R)]$, where A, Δz, and R are the effective area, the out-of-plane displacement and the radius of curvature, respectively. In order to determine the A and R values, we used a simple atomistic model and estimated them by taking into account their variations depending on the "relaxed" displacement z_{rlx} of the closest C atoms. As schematically depicted in Figure 4b, the constituent bond elements playing the leading roles are (i) the three in-plane σ-bonds surrounding the closest C atom when the tip-apex atom is positioned in close proximity over it and make it lifted up by the maximal "relaxed" displacement $z_{\mathrm{rlx}}^{\mathrm{max}}$ and (ii) the six in-plane σ-bonds surrounding the hexagonal ring when the tip-apex atom is directly over the hollow site and $z_{\mathrm{rlx}} = z_{\mathrm{rlx}}^{\mathrm{max(H)}}$. Assuming that the in-plane distortion is negligibly small, the effective area A is expected to be $A_{\mathrm{eff}}^{(C)} = \left(3\sqrt{3}/2\right)a^2\sqrt{1 - (b/2R)^2}$ for the C site and $A_{\mathrm{eff}}^{(H)} = 4A_{\mathrm{eff}}^{(C)}$ for the H site, respectively, where a is the nearest neighbor $C-C$ distance (1.421 A) [39], and b is $\left(\sqrt{3}/2\right)a$. When the tip-apex atom is separated by the equilibrium z_{o} distance ($z_{\mathrm{rlx}} = 0$), where the closest carbon atoms still stay at the original positions, as depicted in the inset of Figure 3b, the effective area A is expected to be equivalent over the central ridge independent of atomically specific sites such as the carbon atoms and hollow sites.

　　　Thereby the "out-of-plane" Young's modulus $E_\perp$ has been evaluated for the C and H sites, and the relationship with their relaxed displacements z_{rlx} is plotted in Figure 4b to examine the dependency on the atomically specific sites. In the case that z_{rlx} is small ($z_{\mathrm{rlx}} < 0.015$ nm), $E_\perp$ is found to be almost constant and similar for the C and H sites, attaining $E_\perp = 10$–13 GPa. This result is in good agreement with previous reports, in which experiments involving nanoindentation and compression of carbon nanotubes by AFM tips were performed and analyzed in the framework of the Hertzian model of continuum mechanics [43]. On the other hand, as z_{rlx} increases further, $E_\perp$ is found to be significantly enhanced ($E_\perp^{\mathrm{max}} > 100$ GPa) for the C site, whereas $E_\perp$ for the H site still stays at a similar value. The increase of the relaxed displacement in the out-of-plane direction would make the carbon atom and its three nearest neighbors no longer planar but instead located in the corners of a pyramid [33]. Such pyramidalization is accounted for by the π-orbital axis vector (POAV) constructions [33,44]. According to the POAV theory, the degree of the valence orbital hybridization is closely correlated to the degree of the relaxed displacement z_{rlx} as follows [33,44]: a slight increment in z_{rlx} leads to a continued stay in a weak π-state with sp^2 hybridization, whereas its further increment yields a transition towards the chemically radical σ-state of a dangling bond with sp^3 hybridization. As mentioned in Section 3.1, the interatomic forces $F_{\mathrm{int}}(z)$ obtained at the H sites have been described solely by Lennard–Jones force, whereas those obtained at the C site have been described by a "hybrid" of Lennard–Jones and Morse forces, corresponding to the sp^2 and sp^3 hybridization. The simulation curve for the C site shows that the contribution of the Morse force (i.e., sp^3 state) remarkably becomes larger with an increase of relaxed displacement z_{rlx}. Intermixing

the σ-state of chemically radical dangling bonds with the non-bonding π-state in the transition from sp^2 to sp^3 hybridization (i.e., π-σ re-hybridization) triggered by the increment of z_{rlx} would explain the obvious enhancement of the "out-of-plane" Young's modulus $E_\perp$ obtained at the C site.

5. Conclusions

Quantitative analysis of the interatomic forces versus tip-sample distance relationships for a hollow carbon nanotube with a well-defined curvature based on 3D-FFS measurements reveals that atomically specific sites representing the depressing and protruding features in surface topography can be assigned to carbon-atom and hollow sites of the honeycomb graphene lattice, respectively. The out-of-plane elastic stiffness at the carbon-atom site was found to become larger than that at the hollow site due to the increase in the "single"-atom displacement for the out-of-plane direction. This phenomenon suggests that sp^2 to sp^3 re-hybridization has been induced by the out-of-plane relaxation of individual carbon atoms in the convexly curved graphene. Our findings allow for a quantitative evaluation of the out-of-plane Young's modulus dependent on the atomically specific sites. The small modulus being almost equivalent at each site supports the validity of continuum mechanics for small out-of-plane relaxation but has been found to increase significantly, with larger relaxation, at individual carbon-atom sites, where sp^2 to sp^3 re-hybridization would take place.

References

1. Lord, E.A.; Mackay, A.L.; Ranganathan, S. *New Geometries for New Materials*, 1st ed.; Cambridge University Press: Cambridge, UK, 2006.
2. Saito, R.; Dresselhaus, G.; Dresselhaus, M.S. *Physical Properties of Carbon Nanotubes*, 1st ed.; Imperial College Press: London, UK, 1998.
3. Dresselhauss, M.S.; Terrones, M. Carbon-Based nanomaterials from a historical perspective. *Proc. IEEE* **2013**, *101*, 1522–1535. [CrossRef]
4. Novoselov, K.S.; Jiang, D.; Schedin, F.; Booth, T.J.; Khotkevich, V.V.; Morozov, S.V.; Geim, A.K. Two-Dimensional atomic crystals. *Proc. Natl. Acad. Sci. USA* **2005**, *102*, 10451–10453. [CrossRef] [PubMed]
5. Nelson, D.; Piran, T.; Weinberg, S. *Statistical Mechanics of Membranes and Surfaces*, 2nd ed.; World Scientific Publishing: Singapore, 2004.
6. Kühnel, W. *Differential Geometry*, 1st ed.; American Mathematical Society: Providence, RI, USA, 2002.
7. Sullivan, J.M. *Discrete Differential Geometry*, 1st ed.; Bobenko, A.I., Schröder, P., Sullivan, J.M., Ziegler, G.M., Eds.; Oberwolfach Seminars; Springer: Berlin, Germany, 2008; Vol. 38.
8. Lee, C.; Wei, X.; Kysar, J.W.; Hone, J. Measurement of the elastic properties and intrinsic strength of monolayer graphene. *Science* **2008**, *321*, 385–388. [CrossRef] [PubMed]
9. Klimov, N.N.; Jung, S.; Zhu, S.; Li, T.; Wright, C.A.; Solares, S.D.; Newell, D.B.; Zhitenev, N.B.; Stroscio, J.A. Electromechanical properties of graphene drumheads. *Science* **2012**, *336*, 1557–1561. [CrossRef] [PubMed]
10. Ortix, C.; Kiravittaya, S.; Schmidt, O.G.; van den Brink, J. Curvature-induced geometric potential in strain-driven nanostructures. *Phys. Rev. B* **2011**, *84*, 045438. [CrossRef]
11. Pacheco Sanjuan, A.A.; Mehboudi, M.; Harriss, E.O.; Terrones, H.; Barraza-Lopez, S. Quantitative chemistry and the discrete geometry of conformal atom-thin crystals. *ACS Nano* **2014**, *8*, 1136–1146. [CrossRef] [PubMed]
12. Geim, A.K.; Novoselov, K.S. The rise of graphene. *Nature Materials* **2007**, *6*, 183–191. [CrossRef] [PubMed]
13. Bonaccorso, F.; Colombo, L.; Yu, G.; Stoller, M.; Tozzini, V.; Ferrari, A.C.; Ruoff, R.S.; Pellegrini, V. Graphene, related two-dimensional crystals, and hybrid systems for energy conversion and storage. *Science* **2015**, *347*, 1246501. [CrossRef] [PubMed]

14. Novoselov, K.S.; Geim, A.K.; Morozov, S.V.; Jiang, D.; Katsnelson, M.I.; Grigorieva, I.V.; Dubonos, S.V.; Firsov, A.A. Two-dimensional gas of massless Dirac fermions in graphene. *Nature* **2005**, *438*, 197–200. [CrossRef] [PubMed]

15. Meyer, J.C.; Geim, A.K.; Katsnelson, M.I.; Novoselov, K.S.; Booth, T.J.; Roth, S. The structure of suspended graphene sheets. *Nature* **2007**, *446*, 60–63. [CrossRef] [PubMed]

16. Fasolino, A.; Los, J.H.; Katsnelson, M.I. Intrinsic ripples in graphene. *Nature Materials* **2007**, *6*, 858–861. [CrossRef] [PubMed]

17. Kim, E.-A.; Castro Neto, A.H. Graphene as an electronic membrane. *Euro. Phys. Lett.* **2008**, *84*, 57007. [CrossRef]

18. Castro Neto, A.H.; Guinea, F.; Peres, N.M.R.; Novoselov, K.S.; Geim, A.K. The electronic properties of graphene. *Rev. Mod. Phys.* **2009**, *81*, 109–162. [CrossRef]

19. Cortijo, A.; Vozmediano, M.A.H. Effects of topological defects and local curvature on the electronic properties of planar graphene. *Nucl. Phys. B* **2007**, *763*, 293–308. [CrossRef]

20. Guinea, F.; Geim, A.K.; Katsnelson, M.I.; Novoselov, K.S. Generating quantizing pseudomagnetic fields by bending graphene ribbons. *Phys. Rev. B* **2010**, *81*, 035408. [CrossRef]

21. San-Jose, P.; González, J.; Guinea, F. Electron-Induced Rippling in Graphene. *Phys. Rev. Lett.* **2011**, *106*, 045502. [CrossRef] [PubMed]

22. Elias, D.C.; Nair, R.R.; Mohiuddin, T.M.G.; Morozov, S.V.; Blake, P.; Halsall, M.P.; Ferrari, A.C.; Boukhvalov, D.W.; Katsnelson, M.I.; Geim, A.K.; et al. Control of graphene's properties by reversible hydrogenation: Evidence for graphane. *Science* **2009**, *323*, 610–613. [CrossRef] [PubMed]

23. Gazit, D. Correlation between charge inhomogeneities and structure in graphene and other electronic crystalline membranes. *Phys. Rev. B* **2010**, *80*, 161406(R). [CrossRef]

24. Boukhvalov, D.W.; Katsnelson, M.I. Enhancement of chemical activity in corrugated graphene. *J. Phys. Chem. C* **2009**, *113*, 14176–14178. [CrossRef]

25. Goler, S.; Coletti, C.; Tozzini, V.; Piazza, V.; Mashoff, T.; Beltram, F.; Pellegrini, V.; Heun, S. Influence of graphene curvature on hydrogen adsorption: Toward hydrogen storage devices. *J. Phys. Chem. C* **2013**, *117*, 11506–11513. [CrossRef]

26. Hickenboth, C.R.; Moore, J.S.; White, S.R.; Sottos, N.R.; Baudry, J.; Wilson, S.R. Biasing reaction pathways with mechanical force. *Nature* **2007**, *446*, 423–427. [CrossRef] [PubMed]

27. Gilman, J.J. Mechanochemistry. *Science* **1996**, *274*, 65–66. [CrossRef]

28. Ashino, M.; Schwarz, A.; Behnke, T.; Wiesendanger, R. Atomic-resolution dynamic force microscopy and spectroscopy of a single-walled carbon nanotube: characterization of interatomic van der Waals forces. *Phys. Rev. Lett.* **2004**, *93*, 136101. [CrossRef] [PubMed]

29. Thess, A.; Lee, R.; Nikolaev, P.; Dai, H.; Petit, P.; Robert, J.; Xu, C.; Lee, Y.H.; Kim, S.G.; Rinzler, A.G.; et al. Crystalline ropes of metallic carbon nanotubes. *Science* **1996**, *273*, 483–487. [CrossRef] [PubMed]

30. Sader, J.E.; Jarvis, S.P. Accurate formulas for interaction force and energy in frequency modulation force spectroscopy. *Appl. Phys. Lett.* **2004**, *84*, 1801–1803. [CrossRef]

31. DeBorde, T.; Joiner, J.C.; Leyden, M.R.; Minot, E.D. Identifying individual single-walled and double-walled carbon nanotubes. *Nano Lett.* **2008**, *8*, 3568. [CrossRef] [PubMed]

32. Ashino, M.; Wiesendanger, R.; Khlobystov, A.N.; Berber, S.; Tománek, D. Revealing subsurface vibrational modes by atom-resolved damping force spectroscopy. *Phys. Rev. Lett.* **2009**, *102*, 195503. [CrossRef] [PubMed]

33. Ashino, M.; Wiesendanger, R. Attractive force-driven superhardening of graphene membranes as a pin-point breaking of continuum mechanics. *Sci. Rep.* **2017**, *7*, 46083. [CrossRef] [PubMed]

34. Horcas, I.; Fernández, R.; Gomez-Rodriguez, J.M.; Colchero, J.; Gómez-Herrero, J.; Baro, A.M. WSXM: A software for scanning probe microscopy and a tool for nanotechnology. *Rev. Sci. Instrum.* **2007**, *78*, 013705. [CrossRef] [PubMed]

35. Ashino, M.; Obergfel, D.; Haluška, M.; Yang, S.; Khlobystov, A.N.; Roth, S.; Wiesendanger, R. Atomically resolved mechanical response of individual metallofullerene molecules confined inside carbon nanotubes. *Nat. Nanotechnol.* **2008**, *3*, 337–341. [CrossRef] [PubMed]

36. Colussi, M.L.; Neves, L.P.; Baierle, R.J. Silicon adsorption in single walled nanotubes. *Braz. J. Phys.* **1991**, *36*, 886–889. [CrossRef]

37. Kittel, C. *Introduction to Solid State Physics*, 6th ed.; John Wiley & Sons Inc.: New York, NY, USA, 1986.

38. Ashino, M.; Wiesendanger, R. Atomic-Resolution dynamic force microscopy/spectroscopy of individual single-walled carbon nanotube. *Jpn. J. Appl. Phys.* **2006**, *45*, 2286–2289. [CrossRef]

39. Dresselhaus, M.S.; Dresselhaus, G.; Saito, R. Physics of carbon nanotubes. *Carbon* **1995**, *33*, 883–891. [CrossRef]

40. Wei, Y.; Wang, B.; Wu, J.; Yang, R.; Dunn, M.L. Bending rigidity and Gaussian bending stiffness of single-layered graphene. *Nano Lett.* **2013**, *13*, 26–30. [CrossRef] [PubMed]

41. Rogers, J.A.; Lagally, M.G.; Nuzzo, R.G. Synthesis, assembly and applications of semiconductor nanomembranes. *Nature* **2011**, *477*, 45–53. [CrossRef] [PubMed]

42. Paulus, G.L.C.; Wang, Q.H.; Strano, M.S. Covalent electron transfer chemistry of graphene with diazonium salts. *Acc. Chem. Res.* **2013**, *46*, 160–170. [CrossRef] [PubMed]

43. Yang, Y.H.; Li, W.Z. Radial elasticity of single-walled carbon nanotube measured by atomic force microscopy. *Appl. Phys. Lett.* **2011**, *98*, 041901. [CrossRef]

44. Haddon, R.C. Hybridization and the orientation and alignment of .pi.-orbitals in nonplanar conjugated organic molecules: .pi.-orbital axis vector analysis (POAV2). *J. Am. Chem. Soc.* **1986**, *108*, 2837–2842. [CrossRef]